Journal of Physiology (2002), **544.3**, *pp.* 741–755
DOI: 10.1113/jphysiol.2002.027490

www.jphysiol.org

Differential exocytosis from human endothelial cells evoked by high intracellular Ca^{2+} concentration

G. Zupančič*, D. Ogden, C. J. Magnus, C. Wheeler-Jones† and T. D. Carter‡

*National Institute for Medical Research, Mill Hill, London NW7 1AA, UK, *University of Ljubljana, Department of Biology, Večna Pot 111, 1001 Ljubljana, POB 2995, Slovenia, †Department of Veterinary Basic Sciences, Royal Veterinary College, Royal College Street, London NW1 0TU, UK and ‡Department of Pharmacology, University College London, Gower Street, London WC1E 6BT, UK*

Endothelial cells secrete a range of procoagulant, anticoagulant and inflammatory proteins by exocytosis to regulate blood clotting and local immune responses. The mechanisms regulating vesicular exocytosis were studied in human umbilical vein endothelial cells (HUVEC) with high-resolution membrane capacitance (C_m) measurements. The total whole-cell C_m and the amplitudes and times of discrete femtoFarad (fF)-sized C_m steps due to exocytosis and endocytosis were monitored simultaneously. Intracellular calcium concentration $[Ca^{2+}]_i$ was elevated by intracellular photolysis of calcium-DM-nitrophen to evoke secretion and monitored with the low-affinity Ca^{2+} indicator furaptra. Sustained elevation of $[Ca^{2+}]_i$ to > 20 μM evoked large, slow increases in C_m of up to 5 pF in 1–2 min. Exocytotic and endocytotic steps of amplitude 0.5–110 fF were resolved, and accounted on average for ~33 % of the total C_m change. A prominent component of C_m steps of 2.5–9.0 fF was seen and could be attributed to exocytosis of von-Willebrand-factor-containing Weibel-Palade bodies (WPb), based on the near-identical distributions of capacitance step amplitudes, with calculated estimates of WPb capacitance from morphometry, and on the absence of 2.5–9.0 fF C_m steps in cells deficient in WPb. WPb secretion was delayed on average by 23 s after $[Ca^{2+}]_i$ elevation, whereas total C_m increased immediately due to the secretion of small, non-WPb granules. The results show that following a large increase of $[Ca^{2+}]_i$, corresponding to strong stimulation, small vesicular components are immediately available for secretion, whereas the large WPb undergo exocytosis only after a delay. The presence of events of magnitude 9–110 fF also provides evidence of compound secretion of WPb due to prior fusion of individual granules.

(Resubmitted 26June 2002 ; accepted after revision 13 August 2002; first published online 6 September 2002).
Corresponding author T. D. Carter: Department of Pharmacology, University College London, Gower Street, London WC1E 6BT, UK. Email: t.carter@ucl.ac.uk

An important function of endothelium is to prevent intravascular coagulation under normal conditions, but to promote blood clotting and inflammation at sites of vessel damage (Mann, 1997). To achieve these opposing functions, endothelial cells secrete several proteins that regulate blood clotting, blood flow and local immune responses. They include procoagulant proteins (e.g. von Willebrand factor (vWf) and Factor VIII), anticoagulant proteins (e.g. tissue plasminogen activator (t-PA), tissue factor pathway inhibitor (TFPI) and Protein S (PS)), and vasoactive and inflammatory proteins (endothelin-1 (ET), calcitonin gene-related peptide (cGRP) and interleukin-8 (IL-8); Stern *et al.* 1986; Wagner, 1990; Schaumburg-Lever *et al.* 1994; Harrison *et al.* 1995; Lupu *et al.* 1995; Emeis *et al.* 1997; Ozaka *et al.* 1997; Russell *et al.* 1998*a*, *b*; Utgaard *et al.* 1998). All these are secreted by exocytosis, the common trigger being an increase in $[Ca^{2+}]_i$, (McNiff & Gil, 1983; Stern *et al.* 1986; Wagner, 1990; Eyden, 1993; Richardson *et al.* 1994; Lupu *et al.* 1995; Emeis *et al.* 1997; Russell *et al.* 1998*b*; Utgaard *et al.* 1998). To understand how the secretion of these differently acting mediators is regulated, it is necessary to determine the time course and dependence on $[Ca^{2+}]_i$ of their release via exocytosis.

The procoagulant vWf is stored in large, specialised granules, the Weibel-Palade bodies (WPb), which are up to 3 μm in length and 0.1–0.2 μm in diameter (Weibel & Palade, 1964, Wagner, 1990). Other inflammatory or coagulant factors, including Factor VIII, cGRP, IL-8 and ET, may be co-localised with vWf in WPb, (Ueda *et al.* 1992; Schaumburg-Lever *et al.* 1994; Ozaka *et al.* 1997; Russell *et al.* 1998*a*, *b*; Utgaard *et al.* 1998). In contrast, anticoagulants including t-PA, PS and TFPI have been localised to separate and much smaller granules, typically less than ~0.25 μm in diameter (Stern *et al.* 1986; Emeis *et al.* 1997; Lupu *et al.* 1997).

Due to their large size, exocytosis of individual WPb may be resolved with high-resolution membrane capacitance (C_m) measurements and may be distinguished from the exocytosis of other, much smaller non-WPb granules. The increase in C_m expected from WPb fusion, calculated from the WPb surface area and a specific C_m of 8 fF μm^{-2}

(Zupančič *et al.* 1994), predicts a mean of 4–5 fF, which is readily detectable with good time resolution by whole-cell recording methods (Neher & Marty, 1982; Fernandez *et al.* 1984; Lindau & Neher, 1988). Anticoagulant-containing secretory granules, for which morphological data exists (Stern *et al.* 1986; Emeis *et al.* 1997; Lupu *et al.* 1997), would be expected to produce unitary events of typically less than 2 fF, close to the limit of resolution of whole-cell recording.

In the study presented here, conventional methods for C_m measurement have been improved to allow detection over a wide range, permitting simultaneous monitoring of total cell C_m and the amplitude and timing of discrete step events during sustained, high elevations of endothelial $[Ca^{2+}]_i$. This allows comparison of the time course and kinetics of WPb fusion with the total C_m change following a $[Ca^{2+}]_i$ increase, to give the time course of WPb and non-WPb exocytosis and endocytosis.

METHODS

Tissue culture

Human umbilical vein endothelial cells (HUVEC) were isolated and grown as described previously (Carter *et al.* 1988). Primary isolates of HUVEC were seeded on to 13 or 35 mm diameter glass coverslips in medium M199 supplemented with 10 % fetal calf serum (FCS), 10 % new born calf serum, 100 U ml^{-1} penicillin and 100 U ml^{-1} streptomycin, and incubated at 37 °C in an atmosphere of 95 % air–5 %CO_2. Cells were used for electrophysiological experiments 4–96 h after isolation.

Immunocytochemistry and measurement of WPb lengths

Cells were washed once in phosphate-buffered saline (PBS; mM: NaCl 136, KCl 2.7, Na_2HPO_4 0.8, KH_2PO_4 1.28, $CaCl_2$ 2, $MgCl_2$ 0.5, pH 7.4) fixed for 20 min in 4 % paraformaldehyde in PBS at room temperature (RT; 25–28 °C), washed five times in PBS and permeabilised for 30 min with 0.1 % Triton-X100 in PBS supplemented with 10 % FCS. Cells were then incubated for 1 h with or without primary antibody (for vWf, 1:200 dilution of mouse anti-human vWf, DAKO; for t-PA, 1:200 dilution of sheep anti-human t-PA, Biogenesis) in PBS supplemented with 1 % FCS. For dual labelling, vWf and t-PA antibodies were added together (1:200 dilution). Cells were then washed five times in PBS and incubated for 1 h with a 1:200 dilution of secondary antibodies (for vWf, donkey anti-mouse Cy2, Jackson Immuno-Research; for t-PA, donkey anti-sheep Cy3, Jackson Immuno-Research), then washed five times in PBS and mounted in non-fluorescent aqueous mountant. Images were acquired with a × 100, 1.35 NA oil-immersion objective (U-PLAN-APO) and Photometrics CH350- cooled CCD camera. Twenty to 30 *Z*-plane sections at 0.2 μm intervals were taken and processed to remove out of focus light with a constrained iterative deconvolution algorithm (Deltavision softWoRx at http://www.api.com). WPb length measurements '*L*' were made from the images of cells stained fluorescently for vWf, and were carried out in ObjectImage (an extended version of NIH image; ftp:/simon.bio.uva.nl/pub). WPb lying in the *X*–*Y* plane (selected by viewing sequential *Z*-plane images) were identified and lengths measured. The mean WPb diameter '*D*' was measured in published electron micrographs (Weibel & Palade, 1964; Elgjo *et al.* 1975; Kagawa & Fujimoto, 1987). The surface area (*S*) was calculated assuming a cylinder diameter, *D*, and length, *L*, with hemispherical ends by the equation:

$$S = \pi D(L + D), \quad (1)$$

WPb *C*m was calculated by multiplying S by a specific *C*m of 8 fF mm^{-2} (determined in melanotrophes; Zupančič et al. 1994). The numbers of WPb granules per cell were counted using ObjectImage (projections of up to 20 0.2 mm sections) in deconvolved fluorescence images of cells stained for vWf. The operator marked WPb granules using a mouse pointer, and a total for the marked sites was stored on computer.

Electrophysiological recording

The whole-cell patch-clamp technique (Hamill *et al.* 1981) was used. Experiments were carried out in a Hepes-buffered physiological saline solution (mM: sodium gluconate 145, potassium gluconate 5, $MgSO_4$ 2, $CaCl_2$ 1.8, glucose 10, Hepes 20, pH 7.4) at RT. Pipette stray capacitance was minimised by coating with molten parafilm (50 % w/w in light mineral oil). Cl^- ions were substituted with gluconate to improve resolution of C_m measurements by reducing C_m changes at high $[Ca^{2+}]_i$. The pipette solution contained (mM): potassium gluconate 110, Hepes 50, $MgSO_4$ 4, Na_2 ATP 4, creatine phosphate 10, pH 7.3 with KOH. Cells were voltage clamped at −50 mV (unless stated otherwise) and current recorded with an Axon Instruments Axopatch 200A amplifier modified to telegraph series resistance and dither the whole-cell capacitance compensation (Axon DC-1 capacitance compensation dither). Data was acquired onto a PC computer using a 16 bit A/D converter (Cambridge Electronic Design CED 1401 plus; in some initial experiments a 12 bit 1401 plus was used). Patch pipettes filled with potassium gluconate solutions had resistances of 1–3 MΩ in external solutions, and access conductances in whole-cell recording were ~150–400 nS.

Fluorescence measurements and flash photolysis

Changes in $[Ca^{2+}]_i$ were measured with furaptra, as described previously (Konishi *et al.* 1991; Ogden *et al.* 1995). Briefly, furaptra (Magfura 2, Molecular Probes; 500 μM) and calcium-DM-nitrophen (synthesised by Gordon Reid, NIMR) were introduced into the cell by diffusion from the patch pipette. Microspectrofluorimetry was performed using a Nikon TMD microscope with a × 40, 1.3 NA objective. Excitation (400–440 nm) was achieved using a 100 W quartz halogen lamp, and emitted light at > 470 nm was detected by a photomultiplier operated in photon-counting mode. Photon counts were converted to an analog signal by a discriminator and an integrating amplifier with correction for missed counts (Cairn Research) and digitised at 1 kHz (CED1401plus, 16 bit, AT bus computer). The method for converting the fluorescence change to free $[Ca^{2+}]_i$ has been described in detail previously (see Ogden *et al.* 1995).

Calcium-DM-nitrophen solutions were prepared and flash photolysis carried out as described previously (Carter *et al.* 1998), with the modification that the flash light was directed into the epifluorescence port of the microscope via a 390 nm dichroic mirror and focussed by the objective to a spot of diameter ~200 μm. DM-nitrophen concentration was measured using the published extinction coefficients (Kaplan & Ellis-Davies, 1988), and the equilibrium free $[Ca^{2+}]$ and $[Mg^{2+}]$ for a given Ca:DM-nitrophen ratio were calculated using the Ca^{2+} and Mg^{2+} dissociation constants for DM-nitrophen (Ellis-Davies *et al.* 1996), ATP (Sillén & Martell, 1971) and furaptra (Konishi *et al.* 1991). Solutions containing 4 mM DM-nitrophen, 4 mM Mg^{2+}, 4 mM ATP and 500 μM furaptra, and either 4 mM or 0 mM Ca^{2+} were

prepared and mixed to vary the Ca:DM-nitrophen ratio. To avoid sudden changes of $[Ca^{2+}]_i$ following membrane rupture in whole-cell recording, internal solutions were prepared with Ca^{2+} and DM-nitrophen concentrations (2.4 mM Ca^{2+} and 4 mM DM-nitrophen) that give a free $[Ca^{2+}]_i$ calculated as 88 nM, similar to the values measured by AM-ester loading of fura-2 or indo-1 in resting HUVEC (70–100 nM; Hamilton & Simms, 1987; Carter *et al.* 1988; Hallam *et al.* 1988).

A single flash applied to a cell loaded with the calcium-DM-nitrophen internal solution resulted in a transient elevation of free $[Ca^{2+}]_i$ that rose to a peak within 1 ms and declined with a half time of ~10 s to resting levels. To maintain $[Ca^{2+}]_i$ at high levels, five or six sequential light pulses at 5 or 10 s intervals were applied. After the last light pulse, the $[Ca^{2+}]_i$ declined approximately exponentially towards pre-flash resting levels. Photolysis light intensity in these experiments produced no bleaching of furaptra fluorescence, and no evidence was found of changes in fluorescence due to the photolysis of DM-nitrophen itself.

C_m measurement

To make a continuous record of capacitance steps and total cell capacitance, the whole-cell capacitance was recalculated at each time point from telegraphs of the series resistance (R_s) and capacitance offsets (C_T). A two-phase lock-in amplifier, constructed to the circuit described by Lindau & Neher (1988), was calibrated to give a 1 V DC output on the two admittance outputs for a 1 V root mean square (r.m.s.) sine input. The zero phase angle of the lock-in amplifier was adjusted as described previously (Carter *et al.* 1998). For whole-cell recordings, 80 mV r.m.s. sinusoidal voltage at 1592 Hz was applied to the pipette. The resulting sinusoidal current was cancelled with the 'slow' transient cancellation circuit of the amplifier (C_{slow}). The extended Lindau & Neher (1988) algorithm (see also Gillis, 1995) was used to calculate the passive cell parameters C_m, membrance conductance (G_m) and access conductance (G_a) from: (1) the two outputs from the phase lock-in amplifier at 0 and −90 degrees (the real and imaginary components of admittance following partial capacitive current cancellation; Y_{Re}, Y_{Im}); (2) telegraphs of the C_{slow} and R_s capacitive current cancellation settings (C_T, R_s); (3) the holding voltage (V_m); and (4) the DC current (I_m). The operation of the C_{slow} and R_s telegraphs is described in Supplementary material on the website:

http://www.jphysiol.org/cgi/content/full/544/3/741

The total Y_{Re} and Y_{Im} components of admittance were found by calculating the real and imaginary parts compensated for by the cancellation controls, telegraphed from the amplifier, and adding the result to the measured outputs of the lock-in amplifier. The total Y_{Re} and imaginary Y_{Im} parts were then used in the Lindau & Neher (L-N) parameter estimation algorithm (Lindau & Neher, 1988) to obtain the total capacitance and conductance. Data were sampled at 1 kHz by the program WinEDR written by Dr John Dempster (University of Strathclyde). I_m, V_m, Y_{Re} and Y_{Im} were low-pass filtered at 100 Hz (−3 dB, 16 pole elliptic) prior to recording. The calculations necessary for parameter estimation and additional filtering were performed offline in MathWorks Matlab. A capacitance dither of 100 fF was applied to the compensation (via an Axon DC-1) to verify 0 deg phase angle and gain settings. The calculated C_m was additionally filtered at 100 Hz (2 × 50th order FIR filter) and DC current (I_{DC}) at 1 Hz (2 × 50th order FIR filter) before step detection. All filtering was done both forward and backward in time to eliminate the distortions due to filter phase shifts.

The L-N algorithm for C_m estimation requires the zero-current potential, V_{rev}, for calculation of G_m. The effect of an erroneous V_{rev} estimate is negligible in low-resolution measurements, especially if G_m is low compared to G_a. However, with the extended L-N algorithm, if V_{rev} is not correctly estimated, a combination of high G_m and high lock-in amplifier gain can produce discontinuities in the C_m trace, and spurious changes of G_m and C_m. To minimise the error, an estimate of V_{rev} was obtained by iteratively adjusting the value of V_{rev} to minimise the difference between C_m values computed before and after a single compensation from a central section of the record. This approach eliminated most discontinuities and produced a substantial noise reduction in the C_m record.

Step detection

The step detection algorithm was essentially as described by Zupančič *et al.* (1994), with the addition of a modified procedure for background noise determination in each 20 s time period analysed; for example see Supplementary material on the website:

http://www.jphysiol.org/cgi/content/full/544/3/741

Briefly, following low-pass filtering (2 × 50th order 100 Hz FIR digital filter), the capacitance record was converted point by point to time derivatives (dC_m/dt). The peak-to-peak (p–p) noise levels, ±3 S.D., were determined as the C_m amplitude corresponding to ±3 S.D. of the dC_m/dt. The procedure was verified empirically under our filtering conditions and assuming white noise, by generating a random noise signal, filtering it at 100 Hz (2 × 50th order FIR filter) and relating ±3 S.D. of amplitude to the ±3 S.D. of the dC_m/dt. The ±3 S.D. of dC_m/dt was obtained by fitting a Gaussian function to the dC_m/dt distribution for each sequential 20 s time frame; only dC_m/dt points within ±2 S.D. of the mean were fitted so as to exclude fast-changing values that might be part of distinct C_m steps. Events that exceeded ±3 S.D. of the Gaussian function fitted to dC_m/dt signal were flagged on the C_m record, and inspected to exclude events associated with large G_a or G_m changes, patch-rupture or bit-level changes in the telegraphs. The amplitude of C_m steps was determined from a phase diagram of dC_m/dt plotted with the amplitude of the C_m changes, as described previously (see Zupančič *et al.* 1994).

Artefacts due to bit-level inaccuracies in the telegraph inputs (C_T and R_S) were minimised by filtering the inputs at 1/50 times the sampling frequency, applying a 50th-order median filter twice to each channel in both directions (forwards and backwards in time), followed by upsampling to the original sampling rate. Further exclusion of artefactual steps was performed by observation during analysis. The false event rate for these records was estimated as 14 per 20 000 points (20 s) from simulated traces of white noise filtered at 100 Hz and processed by the step detection algorithm. The distribution of false steps has a characteristic shape, and amplitudes are much smaller than the nominal detection limit of the algorithm. A theoretical distribution of false-step amplitudes was calculated for each 20 s interval analysed, based on the noise estimate, and any steps falling into this range were excluded (see Zupančič *et al.* 1994).

With this approach, events that have a signal to noise ratio (SNR) of 1 (ratio of amplitude of signal to p–p noise of record) are detected with high reliability and amplitudes can be determined to within 5 % accuracy. The reliability of detecting and accurately estimating event amplitudes decreased with smaller SNRs (e.g. for an SNR of 0.5, 60 % of events are detected and their amplitudes overestimated by ~10 %; see Zupančič *et al.* 1994). During an

experiment the p–p noise may vary. The influence of changes in p–p noise on the resolution and the distribution of p–p noise for the recordings used to construct step-amplitude histograms (Fig. 4) are shown in the Supplementary material on the website:

http://www.jphysiol.org/cgi/content/full/544/3/741

Data are expressed as means ± S.D. unless otherwise stated. Statistical analyses used Student's *t* test, and curve fitting was carried out with maximum likelihood, as described by Colquhoun & Sigworth (1995). Ethical committee approval was obtained for isolation of HUVEC.

RESULTS

Electrical properties of HUVEC in culture

Small endothelial cells that were well separated from neighbouring cells were selected for C_m measurements. The mean ± S.D. C_m, G_a and G_m of the cells recorded was 13.8 ± 3.5 pF (n = 30), 264 ± 70 nS and 1.09 ± 0.9 nS, respectively.

C_m changes evoked by photolysis of calcium-DM-nitrophen in single HUVEC

The effects on C_m of raising $[Ca^{2+}]_i$ are shown in Fig. 1. A single HUVEC of initial C_m ~12 pF was perfused with calcium-DM-nitrophen and furaptra during whole-cell patch-clamp recording. Fig. 1*A*(i) shows the increase in $[Ca^{2+}]_i$ during 17 sequential 1 ms near-UV flashes delivered over 125 s. $[Ca^{2+}]_i$ increased immediately with each flash, declining slightly during the interval, to reach a steady level of ~57 μM in eight flashes. $[Ca^{2+}]_i$ remained at this level during the remainder of the train and declined to the initial level over 2 min when photolysis was stopped. The capacitance traces (Fig. 1*A*(ii)) show that initially, total C_m was declining slowly and the record of the net change due to all detected capacitance steps (C_{det}) was constant. Following elevation of $[Ca^{2+}]_i$, C_m increased by 2.75 pF at a fairly constant rate at high $[Ca^{2+}]_i$, then declined as the free $[Ca^{2+}]_i$ declined. Indicated on the record are the time points when the whole cell capacitence compensation was adjusted (†), and when the phase and

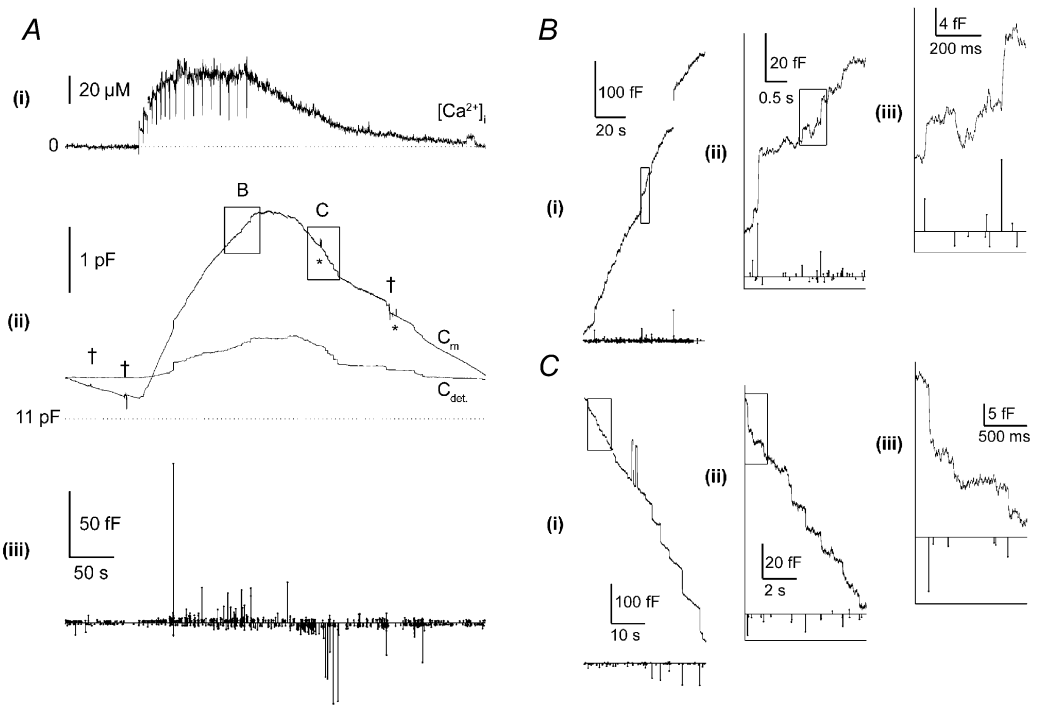

Figure 1. High $[Ca^{2+}]_i$ evokes large increases in membrane capacitance (C_m) that are composed of fast steps in C_m

A, a continuous recording of $[Ca^{2+}]_i$ (i) and C_m (ii) in a single human umbilical vein epithelial cell (HUVEC) that was voltage clamped at a holding potential of 0 mV, and equilibrated with an intracellular solution containing 500 μM furaptra and calcium-DM-nitrophen (2.4:4 mM). At points indicated by the deflections in the Ca^{2+} trace (i), brief (1 ms) pulses of near-UV light were applied (1500 μF, 200 V) from a xenon arc flash lamp. Points at which adjustments were made to the C_m and R_s compensation controls are shown by crosses, and 100 fF dithers of the C_m compensation control via the DC-1 dither module (Axon Instruments) are indicated by * (ii). Superimposed on the C_m trace is the net change in C_m produced by all detected exocytotic and endocytotic events (C_{det}). The time and amplitude of all exocytotic C_m steps (upward lines) and endocytotic C_m steps (downward lines) are shown in (iii). *B*(i) and *C*(i), show regions of C_m and detected steps during a period of strong exocytosis (box *B* in *A*(ii)) and endocytosis (box *C* in *A*(ii)), respectively, on an expanded time scale. *B* or *C* (ii) is the outlined region in (i) expanded, and *B* or *C* (iii) is the outlined region in (ii) expanded. The mean peak-to-peak (p–p) noise during this record was 1.58 ± 0.23 fF.

gain settings were checked (*) by dithering the whole-cell compensation (100 fF).

Many fast steps of C_m attributable to exocytosis and endocytosis can be identified during the rise and fall of $[Ca^{2+}]_i$ in the complete low-gain records shown in Fig. 1*A*(ii). High-gain C_m data in the boxed regions indicated are shown in Fig. 1*B*(i)–(ii) at sequentially higher gains and faster time scale for periods of rapid net exocytosis, and in Fig. 1*C*(i)–(iii) for periods of net endocytosis. These show numerous step increases and decreases of C_m, ranging in amplitude from ~1 to 100 fF. The sum of all the detected C_m steps is shown as a line, C_{det}, in Fig. 1*A*(ii). In this cell, resolved C_m steps account for approximately 25 % of the total C_m change, and the amount of membrane gained in resolved exocytotic steps is lost during the net endocytosis of recovery. Thus, most of the C_m change is due to small events (< ~1 fF), unresolved in this recording. The amplitudes of the resolved C_m steps plotted with time are shown by the vertical lines in Fig. 1*A*(iii). The increase in C_m results from an increase in the frequency and size of exocytotic steps and is analysed in Fig. 7. In contrast, the frequency of endocytotic events increased little compared to baseline during the rising phase of the C_m record, but increased substantially as $[Ca^{2+}]_i$ declined (see also Fig. 7).

Generation and subcellular distribution of WPb, vWf and t-PA

Following plating of dissociated HUVEC, the number of WPb per cell increased with time in culture. Figure 2*A*(i) shows fluorescence images of primary HUVEC labelled with a specific antibody against vWf at 4, 24, 48 and 72 h in culture. At 4 h after plating, few or no WPb could be identified; however, there was strong fluorescence staining due to vWf in perinuclear regions corresponding to endoplasmic reticulum and Golgi apparatus, and patchy staining at the cell/coverslip interface (Fig. 2*A*(i) and *C*(i)).

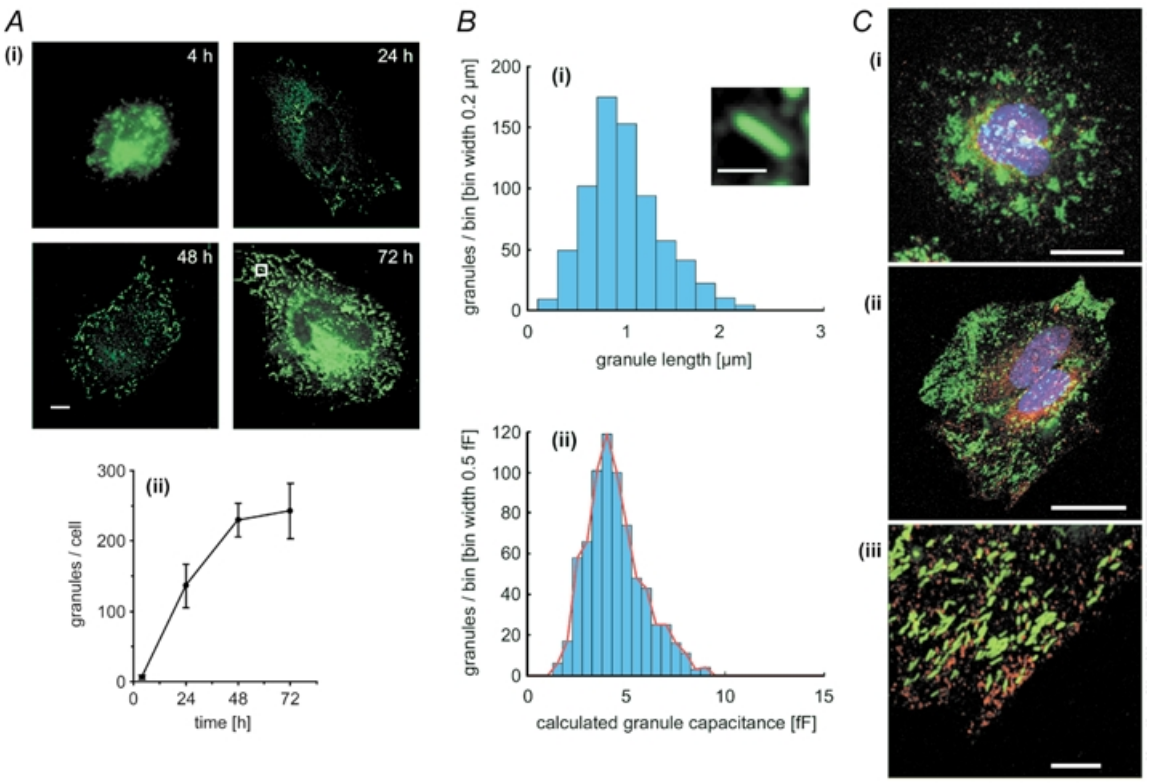

Figure 2. Time-dependent accumulation of Weibel-Palade bodies (WPb), distribution of WPb C_m, and subcellular localisation of von Willebrand factor (vWf) and tissue plasminogen activator (t-PA)

A(i), representative fluorescence images of fixed HUVEC that have been stained with a specific antibody to vWf at the times indicated. Images are projections of three to five, 0.2 μm optical sections, the scale bar indicates 5 μm. The mean number of vWf-immunopositive granules (WPb) counted in 12 cells at each of the indicated times is plotted in (ii) (means ± S.D.). *B*(i), the distribution of lengths of WPb measured from images such as those shown in (i) with an example (inset) of an average WPb from the 72 h cell in *A*(i) (indicated by the white box). The scale bar is 1 μm. The calculated distribution of WPb C_m derived from the data in *B*(i), assuming a specific C_m of 8 fF μm^{-2} is shown in (ii). A red line is drawn through the peak of each bin. *C*(i) and (ii), HUVEC at 4 and 24 h, respectively, labelled with specific antibodies to both t-PA (red) and vWf (green). An expanded region of the image in (ii; – 24 h cell) shows no co-localisation of t-PA and vWf. Images are projections of three, 0.3 μm optical sections, the scale bar being 20 μm in (i) and (ii) and 5 μm in (iii). Nuclear DNA was labelled with Hœchst 33342 (blue).

At 24 h, WPb could be clearly identified, although there was considerable cell-to-cell variability in their numbers, and by 48–72 h in culture, the mean numbers of WPb had reached a steady level (Fig. 2*A*(ii)). Most experiments were made at 48–96 h in culture, although for comparison, some experiments were carried out at 4 h and 24 h (e.g. see Fig. 5).

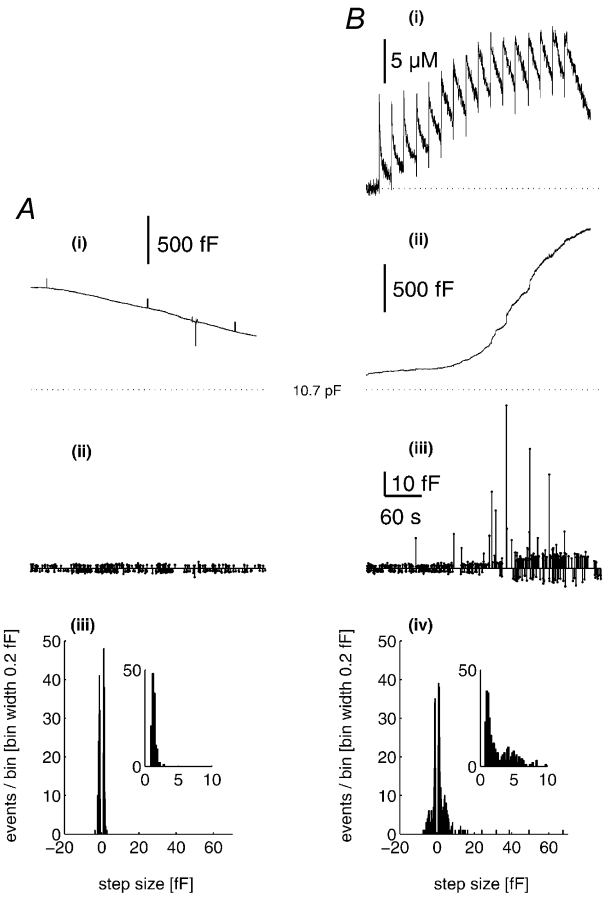

Figure 3. A prominent component of C_m steps with amplitudes in the same range predicted for WPb exocytosis, evoked by high $[Ca^{2+}]_i$

A(i), a continuous record of C_m from an endothelial cell of ~11 pF, voltage clamped at −50 mV and dialysed with a solution containing 500 μM furaptra and calcium-DM-nitrophen (2.4:4 mM). The time and amplitude of discrete C_m steps (exocytotic are indicated by the upward lines, and endocytotic by the downward lines) are shown in *A*(ii). *A*(iii), the amplitude histogram of the detected exocytotic (positive) and endocytotic (negative) events, taken from a 360 s stretch of data. The inset is the exocytotic event amplitude histogram on an expanded scale. The mean p–p noise for the recording was 1.26 ± 0.14 fF. *B*(i) and (ii), continuous records of $[Ca^{2+}]_i$ and C_m, respectively, from similarly sized endothelial cells voltage clamped at −50 mV and dialysed with a solution containing 500 μM furaptra and calcium-DM-nitrophen (2.4:4 mM). Brief (1 ms) pulses of near-UV light (1500 μF, 200 V) were applied at the times indicated by the deflections on the Ca^{2+} record in (i). The time and amplitude of discrete steps in C_m are shown in *A*(iii). *A*(iv), the amplitude histogram of the detected exocytotic and endocytotic steps, taken from a 360 s stretch of data during stimulation. The inset shows the exocytotic events amplitude histogram on an expanded scale. The mean p–p noise of the recording was 1.46 ± 0.36 fF.

Under our culture conditions, t-PA and vWf were stored separately, vWf in large tubular WPb and t-PA in much smaller discrete punctate structures (Fig. 2*C*(i)–(iii)).

Calculation of the capacitance of WPb membranes

The C_m expected for structures of the size and shape of WPb, and their potential contribution to C_m changes was calculated on the basis of morphometric measurements of surface area and specific membrane capacitance. Cross sections of WPb (from electron microscope (EM) studies) are characterised by bundles of hollow tubes or rod-like structures, making their identification unambiguous (e.g. see Wagner, 1990). From 54 measurements of WPb diameters taken from published EM studies (Weibel & Palade, 1964; Elgjo *et al.* 1975; Kagawa & Fujimoto, 1987), the mean ± S.D. WPb diameter, *D*, was estimated as 154 ± 63 nm. The length *L* of 724 WPb was measured from high-resolution deconvolved fluorescence images of endothelial cells stained for vWf. The distribution of lengths is shown in Fig. 2*B*(i). The surface area was calculated (see Methods) and a specific membrane capacitance of 8 fF μm^{-2} (Zupančič *et al.* 1994) applied to yield the calculated distribution of granule capacitance shown in Fig. 2*B*(ii). The distribution ranges from ~2 to 9.0 fF, with a mean of 4.4 ± 1.4 fF. At a C_m step detection resolution of 1.5 fF in the measurements here, > 95 % of WPb exocytosis would be resolved as discrete C_m steps. In contrast, it was calculated that granules containing anticoagulants, which have diameters < 0.25 μm (see Introduction for references), would produce C_m step sizes of less than 2 fF, which is close to, or below the limit of resolution of these recordings.

High $[Ca^{2+}]_i$ triggers exocytosis of WPb

There is evidence to suggest that vWf secretion from WPb requires prolonged high elevated $[Ca^{2+}]_i$, > 10–20 μM (Scrutton & Pearson, 1989; Birch *et al.* 1994), concentrations that are readily achieved during hormone action in endothelial cells in culture and *in situ* (Carter & Ogden, 1994, 1997; Carter *et al.* 1998). We have shown previously that $[Ca^{2+}]_i$ in this range evokes large C_m changes in single HUVEC (Carter *et al.* 1998) and it is of interest to see how individual WPb secretory events are related to the time course of $[Ca^{2+}]_i$ and total C_m changes. Figure 3 shows recordings from two HUVEC of initial capacitance ~11 pF. In the control cell there was no photolytic elevation of $[Ca^{2+}]_i$ (epifluorescence excitation was shuttered; Fig. 3*A*). In the stimulated cell, $[Ca^{2+}]_i$ was increased by photolysis of calcium-DM-nitrophen to levels of > 10 μM (Fig. 3*B*(i)). In the control condition, the total C_m (Fig. 3*A*(i)) declined over 6 min by ~0.5 pF, 4 % of the initial level, and comprised exocytotic and endocytotic steps with approximately equal frequency, and mean amplitude 1.3 fF (Fig. 3*A*(ii)). In the stimulated cell there was a large, slow increase in C_m of > 1 pF, rising slowly immediately after the $[Ca^{2+}]_i$, and then after a delay more rapidly at high $[Ca^{2+}]_i$. An increase in the amplitude and frequency of exocytotic and endo-

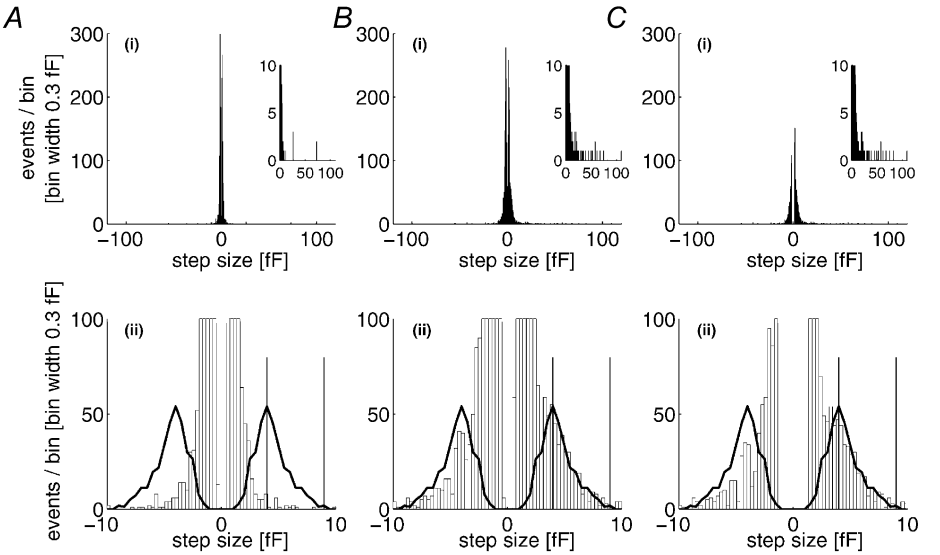

Figure 4. Amplitude histograms for detected C_m steps in unstimulated and high $[Ca^{2+}]_i$ stimulated cells

A(i) and *B*(i), the amplitude histograms for all exocytotic (positive) and endocytotic (negative) events detected during 1900 *s* of recording from four unstimulated cells (mean p–p noise 1.56 ± 0.39 fF; *A*), and 1920 *s* of recording during periods of stimulation by high $[Ca^{2+}]_i$ in eight cells (mean p–p noise 1.56 ± 0.40 fF; *B*). The inset in each case shows the exocytotic events amplitude histogram on an expanded *Y* scale. *A*(ii) and *B*(ii), the same data on expanded *X* and *Y* scales, respectively, with the calculated distribution of WPb C_m superimposed on both the exocytotic and endocytotic distributions. The difference histogram (stimulated − unstimulated), displayed in the same way, is shown in *C*(i) and *C*(ii). The vertical lines on the lower panels indicate the region of the detected C_m steps used to calculate the frequency and kinetics of WPb exocytosis.

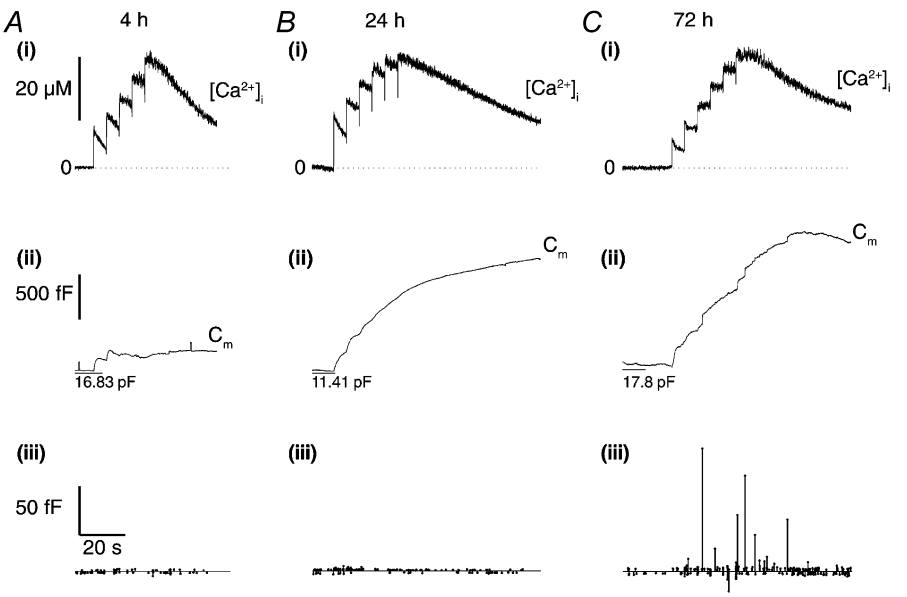

Figure 5. High $[Ca^{2+}]_i$ does not evoke large C_m steps in cells lacking WPb

A(i), *B*(i) and *C*(i), continuous records of $[Ca^{2+}]_i$ in cells at 4, 24 and 72 h post-isolation, respectively. Each cell was voltage clamped at a holding potential of −50 mV, and equilibrated with an intracellular solution containing 500 μM furaptra and calcium-DM-nitrophen (2.4:4 mM) and brief (1 ms) pulses of near-UV light applied (1500 μF, 200 V) at points indicated by deflections in the Ca^{2+} traces. The C_m records are shown in (ii) for each cell, and the amplitudes and times of detected C_m steps (exocytotic are represented by upward lines and endocytotic are represented by downward lines) shown in (iii). The mean p–p noise throughout each recording was 1.60 ± 0.23 fF (*A*), 1.63 ± 0.13 fF (*B*) and 1.91 ± 0.20 fF (*C*).

cytotic steps, and infrequent, large exocytotic C_m steps of 10–60 fF were seen following elevation of $[Ca^{2+}]_i$ (Fig. 3*B*(ii) and (iii)). The data are summarised in the histograms shown in Fig. 3*A*(iii) for the control and Fig. 3*B*(iv) for the stimulated cell. More specifically, the histograms show a component of exocytotic and endocytotic steps in the range ~2–9 fF in the stimulated cell (Fig. 3*B*(iv)) that is absent from control cells, as well as the very large amplitude steps seen in the stimulated cell. Amplitude histograms for exocytotic and endocytotic C_m

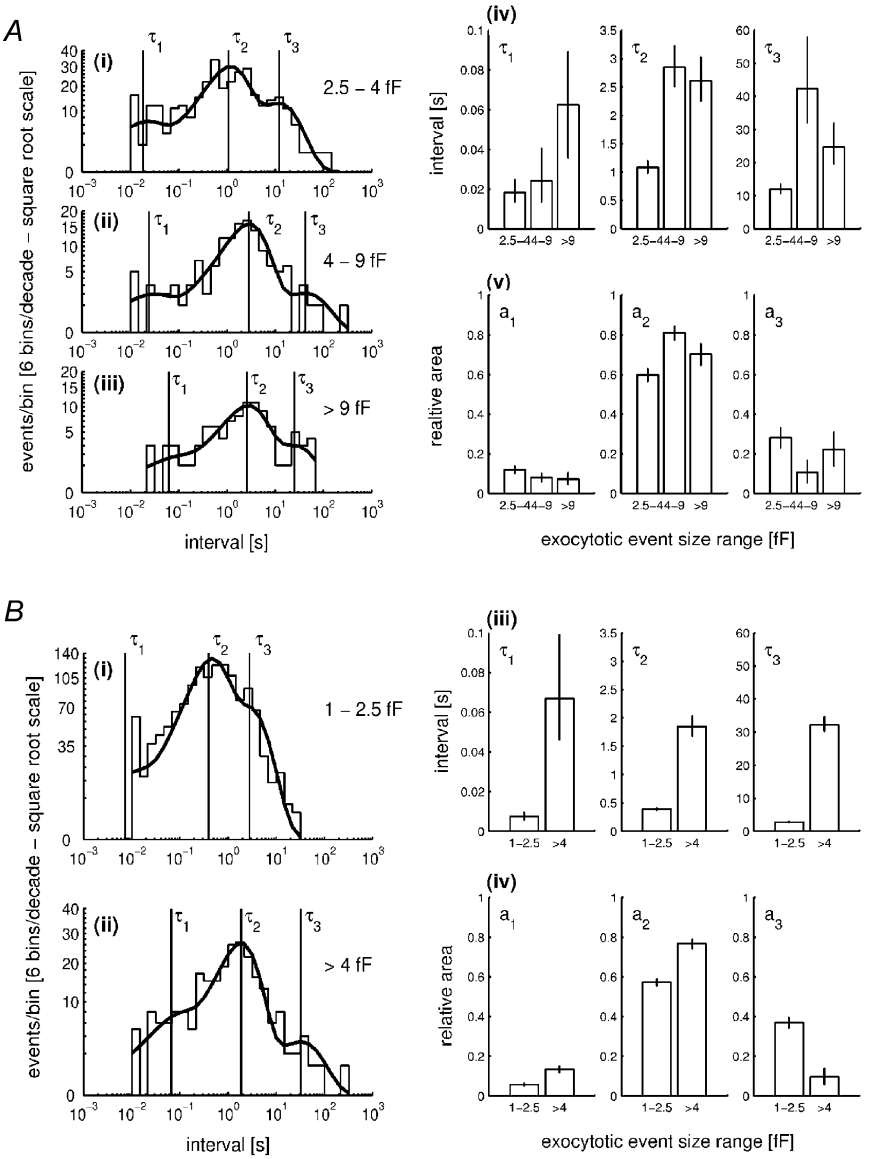

Figure 6. Distribution of intervals between exocytotic events during stimulation by high $[Ca^{2+}]_i$

A, a comparison of interval distributions, plotted as the distribution of the logarithm of the time interval (Sigworth & Sine, 1987), for three subpopulations of exocytotic events: 2.5–4 fF (i), 4–9 fF (ii) and > 9 fF (iii). When generated in this way, an exponential probability density function (p.d.f.) is transformed so that it shows a peak at the value of the time constant. The distributions are limited on the lower end by the filtering bandwidth of 100 Hz (10 ms). Sums of three exponential distributions, with parameters of time constants (τ_1–τ_3) and relative areas (a_1–a_3), were fitted to the data so as to maximise the likelihood of the calculated distribution describing the actual distribution (Colquhoun & Sigworth, 1995). The continuous line shows a calculated sum of three exponential p.d.f. superimposed onto the distribution. Vertical lines indicate the positions of the three time constants. *A*(iv) and (v), a comparison of the parameters of the fitted distributions; time constants (τ_1–τ_3) and relative areas (a_1–a_3), respectively, among the three subpopulations. Vertical error bars correspond to ± −0.5 log likelihood limits. *B*(i) and (ii), the distribution of intervals for events of 1–2.5 and > 4 fF, respectively, produced in the same way as *A*(i)–(iii). *B*(iii) and (iv), a comparison of the parameters of the fitted distributions.

step events derived from 1900 s of data from four control cells, and 1920 s recorded during periods of high $[Ca^{2+}]_i$ in eight cells, are shown in Fig. 4*A*(i) and *B*(i), respectively. The exocytotic amplitude histograms, on a reduced ordinate (inset), show the appearance of infrequent and very large C_m steps in stimulated cells. Figure 4*A*(ii) and *B*(ii) shows, on expanded scales, the amplitude histograms for control and stimulated cells in the ranges predicted for WPb exocytosis. The continuous line shows the distribution of WPb capacitance calculated from the morphometric data of WPb surface areas superimposed on the distribution of C_m steps. There is overlap with a component of events, prominent particularly in stimulated cells. This is shown more clearly by the difference histograms (stimulated − control) plotted in Fig. 4*C*, which shows components of exocytotic and endocytotic events with sizes corresponding to WPb granule capacitance in cells stimulated with high $[Ca^{2+}]_i$.

To test whether the discrete C_m steps with amplitudes in the range predicted for WPb exocytosis were due to WPb, experiments were carried out in cells at early times in culture (4–24 h), when few or no WPb are detectable morphologically (see Fig. 2). At 4 and 24 h, high $[Ca^{2+}]_i$ produced increases in total C_m but with few or no discrete steps in C_m in the range expected for WPb exocytosis (Fig. 5*A* and *B*, respectively). At longer times in culture, when cells have large numbers of WPb, discrete steps in C_m predicted for WPb exocytosis were seen (Fig. 5*C*). Since there are no other large secretory granules in endothelium that could account for these results, and compound fusion of smaller granules is unlikely to produce the distribution of C_m steps observed here, the data taken together suggest that the additional discrete C_m steps, in the range 2–9 fF are due to exocytosis of WPb.

Kinetics of WPb exocytosis

To investigate the kinetics and frequency of WPb exocytosis, events with amplitudes between 4 and 9 fF were identified in the records and attributed to individual WPb fusion based on comparison with the morphometric data shown in Fig. 2*B*(ii) (range indicated in Fig. 4*B*(ii) and *C*(ii) as vertical lines). The lower limit excludes the component of constitutive granule exocytosis that falls in the C_m range calculated for WPbs (Fig. 4*A*(ii)), and contributions from non-WPb-regulated exocytosis; the upper limit excludes the infrequent, very large events that were observed. The distribution of intervals between exocytotic events was measured for amplitudes in three ranges: WPb events of 4–9 fF (Fig. 6*A*(ii)), events of 2.5–4 fF, which are likely to comprise a mixture of constitutive non-WPb granule exocytosis and regulated WPb exocytosis (Fig. 6*A*(i)), and events > 9 fF (Fig. 6*A*(iii)). Each distribution was fitted by maximum likelihood with the sum of three exponential distributions, yielding the best-fit parameters (± −0.5 log likelihood intervals) summarised in Fig. 6*A*(iv) and (v). The similar rates for large granule (> 9 fF) and WPb (4–9 fF) exocytosis, seen by comparing best-fit time constants and areas, indicate that large events and WPb-sized events are components of the same granule population. On this basis, all events of magnitude > 4 fF were pooled (Fig. 6*B*(ii)) and their kinetics compared with events in the size range 1–2.5 fF, which represent predominantly small, non-WPb granule exocytosis (Fig. 6*B*(i)); fitted parameters are shown in Fig. 6*B*(iii) and (iv)). The time constants and areas differ substantially between the two size ranges, with

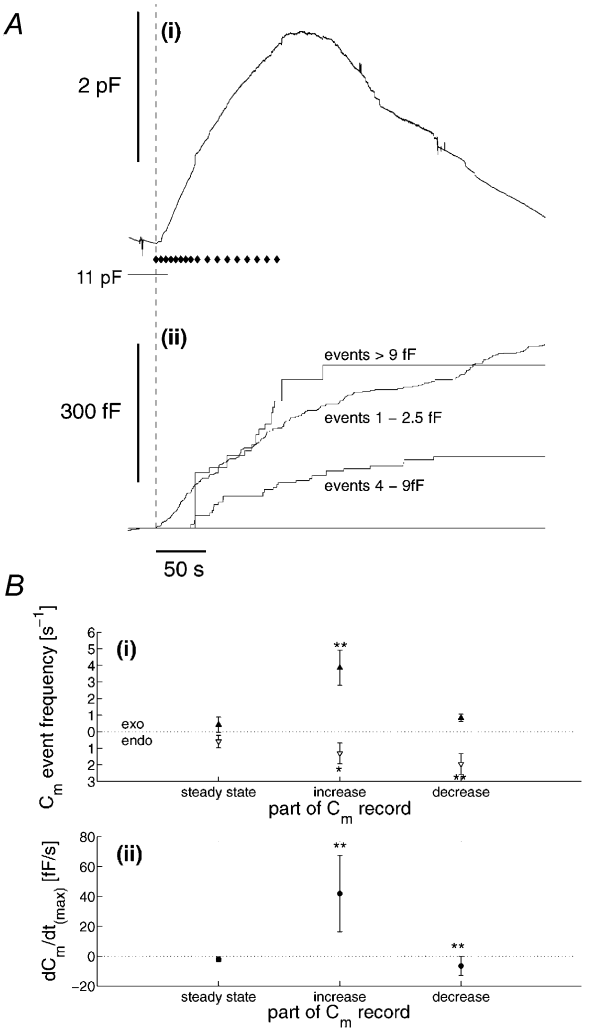

Figure 7. Frequency and time course of granule exocytosis during stimulation by high $[Ca^{2+}]_i$

A(i), the *C*m record for the cell in Fig. 1, with the time points at which light flashes were given indicated ◆. The time of the first flash is indicated by the dashed line. *A*(ii), cumulative plots of *C*m step events 1–2.5 , 4–9 and > 9–fF detected in this record. *B*(i), the mean frequency of all exocytotic (exo; ▲) and endocytotic (endo; △) events for eight cells, determined over a 15 s time window prior to stimulation (steady state), during the steepest part of the increase (increase) or decrease (decrease) in C_m during stimulation. *B*(ii), the mean slope of the C_m record from these regions in the eight cells studied. $^*P = 0.1$, $^{**}P = 0.01$ significance levels, Student's *t* test (determined with respect to the steady-state data).

no overlap of the −0.5 log likelihood regions (Fig. 6*B*(iii) and (iv)), indicating that they are due to different granule populations. Analysis of the distribution of intervals for events in the range 2.5–4 fF showed best-fit parameters intermediate between the small non-WPb events and those for large WPb > 4 fF (Fig. 6*A*(i) and *B*). These parameters may reflect the overlap of WPb exocytosis with constitutive (e.g. Fig. 4*A*(ii)) or non-WPb exocytosis in this size range.

To exclude contributions due to non-WPb exocytosis, the time course of WPb exocytosis was determined using C_m steps in the size range 4–9 fF. This was compared to that for events > 9 fF, which may represent compound secretion of WPb (see below and Discussion), and for events of 1–2.5 fF. The time course of secretion attributed to these three components is shown in Fig. 7*A*, which analyses the data presented in Fig. 1. The exocytotic events in each size range are plotted as cumulative increments of capacitance (Fig. 7*A*(ii)), and compared with the net change of C_m (Fig. 7*A*(i)). In this cell there was a delay of 35 s after the increase in $[Ca^{2+}]_i$ before the first WPb event occurred. A similar delay was seen in the appearance of events > 9 fF, 39 s. In contrast, there was only a short delay in this cell (141 ms) before an increase in total C_m, comprising small or unresolved events due to exocytosis of non-WPb granules. Overall, the delay in WPb and large granule exocytosis was 23.3 ± 7.1 s (n = 8 cells), and 25.2 ± 8.1 s (n = 8 cells), respectively.

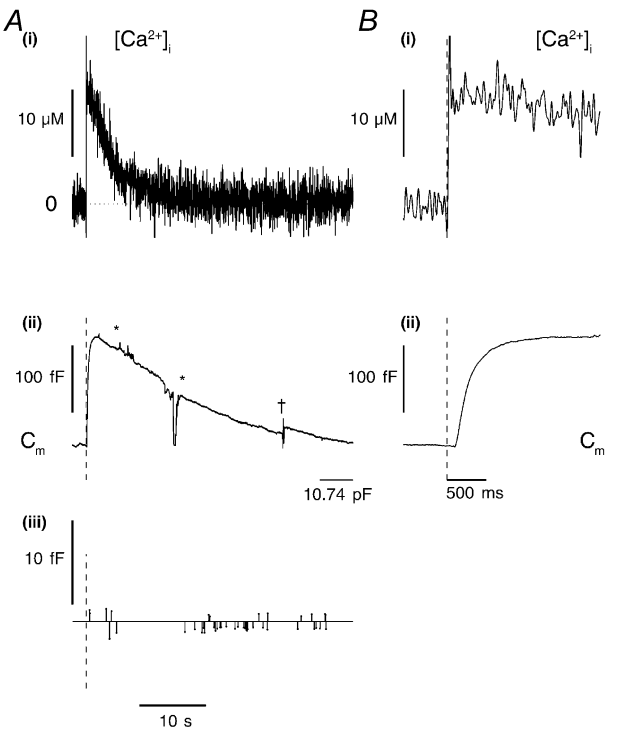

Figure 8. Brief elevation of $[Ca^{2+}]_i$ to high levels does not evoke WPb exocytosis

A, a continuous record of $[Ca^{2+}]_i$ (i) and C_m (ii) from a cell that had been 72 h in culture, voltage clamped at −50 mV and dialysed with a solution containing 500 μM furaptra and calcium-DM-nitrophen (2.4:4 mM). A single, brief (1 ms) pulse of near-UV light (1500 μF, 200 V) was applied at the time indicated by the vertical dashed lines on the records in *A*(ii) and (iii) and *B*(i) and (ii). The detected C_m steps (exocytotic represented by upward lines, and endocytotic by downward lines) are shown in (iii). The area between the stars was excluded from step analysis due to a series of large I_m fluctuations that might have produced spurious changes in C_m. *B*, the early part of the $[Ca^{2+}]_i$ (i) and C_m (ii) response on an expanded time scale. The p–p noise was 0.88 ± 0.30 fF for the period shown. †, the point at which a C_T and R_s compensation was applied.

Contribution of exocytotic and endocytotic events to total C_m changes

In control cells, C_m declined slowly at a rate of 2.2 ± 2.7 fF s^{-1} (n = 4 cells). The overall frequency of exocytotic and endocytotic events detected was 0.87 and 1.07 events s^{-1}, respectively. Events falling in the range 4–9 fF, reflecting basal WPb exocytosis, occurred much less frequently (0–0.033 events s^{-1}).

In cells with high $[Ca^{2+}]_i$ due to photolysis, the frequency of C_m steps was determined for 15 s time windows in three parts of the response: (a) at rest just prior to stimulation, (b) during the steepest part of the increase in C_m and (c) during the steepest period of the C_m decrease. The results are summarised in Fig. 7*B*(i). Prior to stimulation, C_m declined at a mean rate of 2.0 ± 1.6 fF s^{-1}, and the frequencies of exocytotic and endocytotic events were similar. Following elevation of $[Ca^{2+}]_i$, C_m increased with a mean rate of 41.8 ± 9.6 fF s^{-1}, as shown in Fig. 7*B*(ii), coincident with a large increase in the frequency of exocytotic events and a smaller increase in frequency of endocytotic events (Fig. 7*B*(i)). During this period, the frequency of events of amplitude 4–9 fF, attributed to WPb exocytosis, increased to between 0.1 and 1.8 events s^{-1}. Finally, in cells in which the C_m declined as $[Ca^{2+}]_i$ declined to pre-flash levels, the frequency of exocytotic events decreased to close to pre-flash levels, whereas the frequency of endocytotic events increased (five cells; Fig. 7*B*(i)). These results indicate that most of the rapid increase in C_m during stimulation is due to a large increase in the frequency of exocytosis, and that increased endocytosis and decreased exocytosis result in the decline of C_m. The almost symmetrical distributions of exocytotic and endocytotic event amplitudes shown in the histogram of Fig. 4*C*(ii) show that the step sizes detected and the numbers in each bin range are similar for exocytosis and endocytosis, implying that similar membrane areas are gained and lost in single exocytotic and endocytotic events.

In eight cells, the mean contribution to the C_m change, after correction for detected endocytosis, from exocytosis of WPb granules in the 4–9 fF range was 6.0 %, and for granules > 9 fF, 14.4 %. For detected exocytotic events of magnitude < 4 fF thought to include both non-WPb and a

proportion due to WPb, this was 14.5 %. The remaining 65 % comprises the net exocytosis and endocytosis of unresolved granules.

Exocytosis during brief elevations of $[Ca^{2+}]_i$

Following a single flash producing a rise of $[Ca^{2+}]_i$ there was often a small (45–433 fF, $n = 17$) rapid increase in C_m, containing a few detected steps typically less than ~2 fF in amplitude. The time course of this early increase comprises a delay in the range 13–174 ms ($n = 17$), a fast rise with a maximum rate of change of C_m of 337 fF s^{-1} (range 34–337 fF s^{-1}, $n = 17$), followed by a slower decline. In the record shown in Fig. 8, C_m increased after a delay of 93 ms, peaked 1.59 s after the maximum $[Ca^{2+}]_i$, and subsequently declined to pre-flash levels over 13 s. The region marked between the asterisks in Fig. 8*A*(ii) was excluded from analysis because of large I_m excursions that might have produced spurious changes in the C_m record. No C_m steps of the amplitude expected for WPb exocytosis were detected (Fig. 8*A*(iii)).

DISCUSSION

An elevation of $[Ca^{2+}]_i$ is known to be a strong stimulus for secretion in vascular endothelial cells (Stern *et al.* 1986; Hamilton & Sims, 1987; Scrutton & Pearson, 1989; Birch *et al.* 1992, 1994; Kooistra *et al.* 1994; Frearson *et al.* 1995; Lupu *et al.* 1995; Carter & Ogden, 1997), and produces a large increase (up to 30 %) in endothelial C_m (Carter *et al.* 1998). In this study we show that the changes in endothelial C_m resulting from high $[Ca^{2+}]_i$ comprise discrete step changes in C_m due to exocytosis and endocytosis. The resolution of these recordings permitted detection of C_m steps typically > 1.5 fF, sufficient to resolve more than 95 % of events due to fusion of WPb granules, as well as some events due to small non-WPb granule exocytosis, and further showing that a large proportion of the C_m change is due to secretory events < 1.5 fF in size. The results provide evidence that a major component of the distribution of C_m steps detected is due to exocytosis of WPb. Identification of this component shows a long delay, > 20 s, in the time course of WPb exocytosis evoked by $[Ca^{2+}]_i$ elevation, and contrasts with the immediate C_m increase due to small granule exocytosis.

Ca^{2+} concentration and vascular secretion

In the experiments described here, exocytosis of WPb required free $[Ca^{2+}]_i$ levels typically of 10–60 μM. Although high, these levels of free $[Ca^{2+}]_i$ are comparable to those recorded during hormonally evoked responses. Secretion of anticoagulants such as t-PA occurs rapidly following stimulation, and is triggered by the first phase of the hormone-evoked $[Ca^{2+}]_i$ elevation (Kooistra *et al.* 1994; Lupu *et al.* 1995), comprising a transient increase in $[Ca^{2+}]_i$ to between 7 and 30 μM, due to InsP_3-evoked Ca^{2+} release from internal stores (Carter & Ogden, 1994, 1997; Carter *et al.* 1998). Local $[Ca^{2+}]_i$ in domains close to calcium-release sites are likely to be much higher than these averaged levels (Carter & Ogden, 1994, 1997). Brief increases of $[Ca^{2+}]_i$ in this range produced by hormone, or by photolysis of caged InsP_3 or caged Ca^{2+} evoked small increases of C_m (Carter *et al.* 1998). During this phase of the exocytotic response, only small discrete C_m events (less than 2.5 fF) can be resolved, indicating net exocytosis of small granules or vesicles only (Fig. 8). On the other hand, secretion of vWf from intact endothelial cells has been shown to require prolonged elevation of $[Ca^{2+}]_i$ or frequent prolonged periods of Ca^{2+} spiking (Birch *et al.* 1994). In permeabilised endothelial cells, maximal vWf secretion was shown to require $[Ca^{2+}]_i$ > 10–20 μM (Scrutton & Pearson, 1989; Birch *et al.* 1992). The data presented here and that reported by Carter *et al.* (1998) show that similar high levels of $[Ca^{2+}]_i$ are required to evoke large overall increases in endothelial C_m.

Identification of C_m steps due to WPb exocytosis

On the basis of morphometric measurements of membrane area, WPb granules are predicted to contribute C_m steps of amplitude between ~2 and 9 fF (mean 4.4 fF) if membrane fusion occurs in a concerted event. Here we show that the increase in C_m produced by maintained high $[Ca^{2+}]_i$ contains steps ranging in amplitude from ~1.0 to 100 fF, with a prominent component in the range ~2–9 fF similar to that predicted for WPb fusion. C_m steps in this range of amplitudes are absent in recordings from cells at 4 h in culture that have no WPb, and are present in recordings from cells 1–3 days in culture that have developed immunocytochemically identified WPb. These results suggest strongly that the additional C_m steps in stimulated cells, in the range 2–9 fF, are due to WPb exocytosis. In resting cells, C_m events in the range 4–9 fF, corresponding to the upper range of WPb sizes, were infrequent (0–0.033 events s^{-1}). Following stimulation, the frequency of events in this size range increased to a maximum of 1.8 events s^{-1}, indicating that prolonged high $[Ca^{2+}]_i$ evokes a large increase in WPb exocytosis, as predicted by biochemical studies of vWf secretion (Scrutton & Pearson, 1989; Birch *et al.* 1994).

Delays in small granule and WPb exocytosis

Following an abrupt increase of $[Ca^{2+}]_i$, there was a short delay (minimum 13 ms) before an increase in C_m occurred. During the early part of the increase, the few exocytotic steps of C_m detected were typically 1–2 fF in amplitude, indicating that exocytosis of small granules (< 0.25 μm in diameter) predominates early in the response. A further elevation of $[Ca^{2+}]_i$ within a few seconds of the first resulted in an additional fast increase in C_m, again comprising small C_m steps (e.g. Figs 1, 5 and 7). These results indicate that WPb exocytosis does not occur early in the response to high $[Ca^{2+}]_i$ and that small granules are readily available for exocytosis following a fast increase of $[Ca^{2+}]_i$ produced

by the first or a subsequent flash. The small granules comprising this phase of the C_m change may include those containing anticoagulants such as t-PA, TFPI and PS (Stern *et al.* 1986; Emeis *et al.* 1997; Lupu *et al.* 1997), which are known to be secreted rapidly in response to a rise in $[Ca^{2+}]_i$ (Stern *et al.* 1986; Kooistra *et al.* 1994; Lupu *et al.* 1995). Evidence was also obtained that small granule secretion continues to predominate during prolonged $[Ca^{2+}]_i$ elevations in which most of the C_m change (> 65 %) is due to small or unresolved exocytotic and endocytotic events.

In contrast to the small granule secretion, the delay between the rise of $[Ca^{2+}]_i$ and the first large C_m steps attributable to WPb exocytosis was long, with a mean of 23 s. Furthermore, the overall rate of exocytosis of WPb is slow when compared with other tissues (Henkel & Almers, 1996), suggesting that multiple steps may be involved in WPb exocytosis. Further evidence of this was obtained here in the distribution of intervals between C_m steps. When partitioned into amplitude ranges 1–2.5, 2.5–4, 4–9 and > 9 fF, the distribution of intervals were in each case fitted with the sum of three exponential components, indicating that several steps in the secretory process are initiated by high $[Ca^{2+}]_i$. In the two ranges 4–9 and > 9 fF, the time constants and amplitudes of the components determined by maximum likelihood were similar, consistent with the expectation that large events (> 9 fF), arise from the WPb pool of granules. The slowest time constant in the distribution of intervals was similar to the delay seen in WPb and large granule exocytosis after rapid elevation of $[Ca^{2+}]_i$, consistent with a slow step of 20–30 s in the Ca^{2+} activation of WPb exocytosis. In contrast, events < 2.5 fF showed a substantially different distribution of intervals, indicating different processes in the calcium-evoked secretion of small non-WPb granules. In the range 2.5–4 fF, the distribution was intermediate between the small events and events > 4 fF, most probably comprising a mixture of regulated WPb exocytosis, and a component of basal or constitutive granule exocytosis. Histological studies indicate that anticoagulant-containing granules are typically < 0.25 μm in diameter (Stern *et al.* 1986; Emeis *et al.* 1997; Lupu *et al.* 1997); however, the lack of detailed analysis of the distribution of sizes of anti-coagulant granules leaves open the possibility that some may be large enough to contribute to events in the range 2.5–4 fF. Evidence of a long delay in WPb exocytosis has been reported elsewhere. vWf-dependent platelet adhesion to venular endothelium *in vivo* occurs with a delay of 20–30 s following stimulation with histamine or ionophore (Andre *et al.* 2000). Using atomic-force microscopy (albeit in post-stimulation, fixed tissue), Schneider *et al.* (2000) reported numerous 200–500 nm diameter, ring-like structures in the plasmalemma, 30–50 s after stimulation with a protease-activated receptor 2 agonist, which they suggested reflected WPb exocytosis. The function of the slow step in producing the delay in WPb secretion may be to limit procoagulant or inflammatory-mediator release following brief stimulation, at the same time allowing the anticoagulant secretions from small granules and other non-vesicular mechanisms necessary for preventing intra-vascular coagulation, the main homeostatic function of endothelium.

Differential secretion from several granule populations in the same cell is achieved by many tissues. For example, neutrophils involved in regulating local immune responses contain several different storage granules that are exocytosed in a co-ordinated fashion. Secondary and tertiary granules are exocytosed in response to low levels of elevated $[Ca^{2+}]_i$, and peroxidase-positive, primary granules are released at much higher $[Ca^{2+}]_i$ (Nusse *et al.* 1998). In neutrophils and other cells (Verhage *et al.* 1991), it has been suggested that different Ca^{2+} sensitivities of the granule populations may provide a basis for this regulation. The details of the mechanisms and their similarities with endothelium remain to be established.

Large C_m steps

A significant proportion of the C_m change evoked by high $[Ca^{2+}]_i$ is attributable to very large (> 9 fF) step increases in C_m that cannot be accounted for by individual WPb or other endothelial secretory granules. Large C_m steps have been reported in a number of different cells during stimulation with high $[Ca^{2+}]_i$, and arise either because the individual secretory granules themselves are very large (e.g. the beige mouse mast cell; Breckenridge & Almers, 1987), or from the compound fusion of several smaller granules prior to or during exocytosis (e.g. eosinophil secretion; see Scepek & Lindau, 1993). In some cell types the nature of the exocytosed compartment is not clear, although one possible candidate is the lysosome (reviewed in Andrews, 2000).

Several lines of evidence suggest that the large steps seen here are due to compound fusion of WPb. First, the presence of large C_m steps at high $[Ca^{2+}]_i$ correlates with the development of WPb; they were not seen in cells lacking WPb, appearing only in cells at > 24 h in culture when WPb are well established (e.g. Fig. 5*C*). Second, the large C_m events seen here have the same kinetics of secretion as the well-defined 4–9 fF WPb component of exocytotic steps, showing a long delay and similar time constants and amplitudes in the distribution of intervals (Fig. 6*A*). The long delay in WPb exocytosis (tens of seconds) would provide sufficient time for fusion of multiple WPb prior to exocytosis. Third, morphological studies suggest that following cell stimulation, WPb undergo compound fusion to form large vacuolar structures prior to exocytosis (Fujimoto, 1982; Richardson *et al.* 1994). Alternative explanations for these large C_m steps include the exocytosis of some other large compartment such as lysosomes (Andrews, 2000), or the compound fusion of many small

non-WPb granules. Lysosomal exocytosis may occur in endothelium (De Bruyn & Cho, 1986), and recent results in other tissues have linked calcium-triggered lysosomal fusion or compound fusion of intracellular vesicles in the resealing of disrupted plasma membrane (McNeil & Steinhardt, 1997; Terasaki *et al.* 1997). However, in the experiments reported here it is unlikely that exocytosis of lysosomes or compound fusion of smaller bodies accounts for the large steps. Lysosomes are present in freshly isolated endothelial cells and at 24 h in culture, but large C_m steps were not seen in these cells, although overall net C_m changes in response to high $[Ca^{2+}]_i$ were seen due to the cumulative secretion of small secretory bodies (e.g. Fig. 5*A*, *B*). The evidence presented here favours the compound fusion of WPb as an explanation of the large steps of C_m during high $[Ca^{2+}]_i$. Compound fusion may provide a mechanism by which it is possible to increase the efficiency of delivery of vWf, P-selectin and membrane to the cell surface under conditions of strong or prolonged stimulation.

Endocytosis

In resting cells, endothelial C_m declines slowly (at ~2 fF s^{-1}) during whole-cell recording. Similar observations have been made in many other cell types (Neher & Marty, 1982; Almers & Neher, 1987; Gillis & Miser, 1993; Burgoyne & Handel, 1994; Zupančič *et al.* 1994), and the reasons for the decline are not clear. Separation of detected exocytotic and endocytotic steps in resting endothelial cells showed a slightly higher frequency of endocytotic events (Fig. 7*B*), indicating that the slow decline is most probably due to a net endocytosis of membrane. Although care was taken to ensure that no large changes in resting $[Ca^{2+}]_i$ occurred during patch-clamp recording, other factors such as the loss by dialysis of the small cell components required to maintain resting rates of exocytosis and endocytosis cannot be ruled out. However, evidence that the endocytotic machinery was not significantly disrupted under our experimental conditions was provided by the ability of many cells (5/8) to retrieve most if not all of the additional membrane inserted by exocytosis following stimulation.

Following elevation of $[Ca^{2+}]_i$ there was an increase in the frequency of endocytotic events, often less pronounced during the early phase of the rise in $[Ca^{2+}]_i$, but increasing after periods of strong exocytosis as $[Ca^{2+}]_i$ declined. The amplitude of endocytotic steps during the latter phase were often large (up to ~60 fF), similar to those reported in a number of other cell types following periods of exocytosis triggered by high $[Ca^{2+}]_i$ (reviewed in Henkel & Almers, 1996). This retrieval mechanism is thought to require high $[Ca^{2+}]_i$, and may involve a dynamin rather than a clathrin-mediated mechanism (Henkel & Almers, 1996). An increased frequency of endocytotic steps similar in amplitude to WPb exocytotic events in stimulated cells (Fig. 4*C*) raises the possibility that the WPb membrane may be retrieved by a cavity recapture (cavicapture) mechanism (see Henkel & Almers, 1996).

Conclusions

In endothelial cells, large changes in C_m evoked by prolonged high $[Ca^{2+}]_i$ are composed of many discrete steps in C_m. A component of these C_m steps of amplitude 2.5–9 fF was identified as WPb exocytosis. The results indicate that ~20 % of the membrane area increase is due to net WPb exocytosis, and > 65 % is due to small granule secretion. The time course of WPb exocytosis includes a delay of approximately 20 s with respect to the $[Ca^{2+}]_i$ rise, whereas the secretion of small granules that may contain several important anticoagulant mediators, increases immediately. The delay in WPb exocytosis may provide a mechanism to prevent inflammatory mediator release during brief low-level stimulation, while allowing secretion of anticoagulants for the prevention of blood clotting. At sites of vascular injury or inflammation there is likely to be a strong or prolonged activation of endothelial cells, conditions favouring the exocytosis of WPb and the delivery of vWf and P-selection to promote blood clotting and an inflammatory response.

REFERENCES

Andre, P., Denis, C. V., Ware, J., Saffaripour, S., Hynes, R. O., Ruggeri, C. M. & Wagner, D. D. (2000). Platelets adhere to and translocate on von Willebrand factor presented by endothelium in stimulated vein. *Blood* **96**, 3322–3328.

Andrews, N. W. (2000). Regulated secretion of conventional lysosomes. *Trends in Cell Biology* **10**, 316–321.

Almers, W. & Neher, E. (1987). Gradual and stepwise changes in the membrane capacitance of rat peritoneal mast cells. *Journal of Physiology* **386**, 205–217.

Birch, K. A., Pober, J. S., Zavoico, G. B., Means, A. R. & Ewenstein, B. M. (1992). Calcium/calmodulin transduces thrombin-stimulated secretion: studies in intact and minimally permeabilised human umbilical vein endothelial cells. *Journal of Cell Biology* **118**, 1501–1510.

Birch, K. A., Ewenstein, B. M., Golan, D. E. & Pober, J. S.(1994). Prolonged peak elevations in cytoplasmic free calcium ions, derived from intracellular stores, correlate with the extent of thrombin-stimulated exocytosis in single human umbilical vein endothelial cells. *Journal of Cellular Physiology* **160**, 545–554

Breckenridge, L. J. & Almers, W. (1987). Final steps in exocytosis observed in a cell with giant secretory granules. *Proceedings of the National Academy of Science of the USA* **84**, 1945–1949.

Burgoyne, R. D. & Handel, S. E. (1994). Activation of exocytosis by GTP analogues in adrenal chromaffin cells revealed by patch-clamp capacitance measurement. *FEBS Letters.* **344**, 139–142.

Carter, T. D., Hallam, T. J., Cusack, N. J. & Pearson, J. D. (1988). Regulation of P2y-purinoceptor-mediated prostacyclin release from human endothelial cells by cytoplasmic calcium concentration. *British Journal of Pharmacology* **95**, 1181–1190.

Carter, T. D. & Ogden D. (1994). Acetylcholine-stimulated changes of membrane potential and intracellular Ca^{2+} concentration recorded in endothelial cells in situ in the isolated rat aorta. *Pflügers Archiv* **428**, 476–484.

Carter, T. D. & Ogden, D. (1997). Kinetics of Ca^{2+} release by InsP3 in pig single aortic endothelial cells: evidence for an inhibitory role of cytosolic Ca^{2+} in regulating hormonally evoked Ca^{2+} spikes. *Journal of Physiology* **504**, 17–33.

Carter, T. D. & Pearson, J. D. (1992). Regulation of prostacyclin synthesis in endothelial cells. *News in Physiological Sciences* **7**, 64–69.

Carter T. D., Zupančič, G., Smith, S. M., Wheeler-Jones, C. & Ogden, D. (1998). Membrane capacitance changes induced by thrombin and calcium in single endothelial cells cultured from human umbilical vein. *Journal of Physiology* **513**, 845–855.

Colquhoun, D. & Sigworth, F. J. (1995). Fitting and statistical analysis of single-channel records. In *Single Channel Recording*, 2nd edn, eds Sakmann, B. & Neher, E., pp. 483–587. Plenum, New York.

De Bruyn, P. P. & Cho, Y. (1986). *In vivo* exocytosis of lysosomes by the endothelium of the venous sinuses of bone marrow and liver: visualization at normal and low body temperature. *American Journal of Anatomy* **177**, 35–41.

Elgjo, R. F., Henriksen, T. & Evensen, S. A. (1975). Ultrastructural identification of umbilical cord vein endothelium in situ and in culture. *Cell Tissue Research* **162**, 49–59.

Ellis-Davies, G. C. R., Kaplan, J. H. & Barsotti, J. R. (1996). Laser photolysis of caged calcium: rates of calcium release by nitrophenyl-EGTA and DM-nitrophen. *Biophysical Journal* **70**, 1006–1016.

Emeis, J. J., Van Den Eijnden-Schrauwen, Y., Van Den Hoogen, C. M., De Priester, W., Westmuckett, A., Lupu, F. (1997). An endothelial storage granule for tissue-type plasminogen activator. *Journal of Cell Biology* **139**, 245–256.

Eyden, B. P. (1993). Ultrastructural observations on Weibel-Palade bodies suggesting exocytosis. *Journal of Submicroscopic Cytology and Pathology* **25**, 145–148.

Fernandez, J. M., Neher, E. & Gomperts, B. D. (1984). Capacitance measurements reveal stepwise fusion events in degranulating mast cells. *Nature* **312**, 453–455

Frearson, J. A., Harrison, P., Scrutton, M. C. & Pearson, J. D. (1995). Differential regulation of von Willebrand factor exocytosis and prostacylin synthesis in electro-permeabilised endothelial cell monolayers. *Biochemical Journal* **309**, 473–479.

Fujimoto S. (1982). Degranulation of endothelial specific granules of the toad aorta after treatment with compound 48/80. *Anatomical Records* **203**, 197–204.

Gillis K. D. (1995). Techniques for membrane capacitance measurements. In *Single Channel Recording*, 2nd edn., ed Sakmann, B. & Neher, E, pp. 155–197. Plenum, New York.

Gillis, K. D. & Misler, S. (1993). Enhancers of cytosolic cAMP augment depolarization-induced exocytosis from pancreatic B-cells: evidence for effects distal to Ca^{2+} entry. *Pflügers Archive* **424**, 195–197.

Hallam, T.J., Pearson, J. D. & Needham, L. (1988). Thrombin-stimulated elevation of endothelial cell cytoplasmic free calcium concentration causes prostacylin production. *Biochemical Journal* **257**, 243–249.

Hamill, O. P., Marty, A., Neher, E., Sakmann, B. & Sigworth, F. J. (1981). Improved patch-clamp techniques for high-resolution current recording from cells and cell-free membrane patches. *Pflügers Archiv* **391**, 85–100.

Hamilton, K. K. & Sims, P. J. (1987). Changes in cytosolic Ca^{2+} associated with von Willebrand factor release in human endothelial cells exposed to histamine. Study of microcarrier cell monolayers using the fluorescent probe indo-1. *Journal of Clinical Investigation* **79**, 600–608.

Harrison, V. J., Barnes, K., Turner, A. J., Wood, E., Corder, R. & Vane, J. R. (1995). Identification of endothelin-1 and big endothelin-1 in secretory vesicles isolated from bovine aortic endothelial cells. *Proceedings of the National Academy of Science of the USA* **92**, 6344–6348.

Henkel A. W. & Almers W. (1996). Fast steps in exocytosis and endocytosis studied by capacitance measurements in endocrine cells. *Current Opinion in Neurobiology* **6**, 350–357.

Kagawa, H. & Fujimoto, S. (1987). Electron-microscopic and immunocytochemical analyses of Weibel-Palade bodies in the human umbilical vein during pregnancy. *Cell Tissue Research* **249**, 557–563.

Kaplan, J. H. & Ellis-Davies, G. C. (1988). Photolabile chelators for the rapid photorelease of divalent cations. *Proceedings of the National Academy of Science of the USA* **85**, 6571–6575.

Konishi, M., Hollingworth, S., Hawkins, A. B. & Baylor, S. M.(1991). Myoplasmic Ca transients in intact frog skeletal muscle fibres monitored with the fluorescent indicator furaptra. *Journal of General Physiology* **97**, 271–302.

Kooistra, T., Schrauwen, Y., Arts, J. & Emeis, J. J. (1994). Regulation of endothelial cell t-PA synthesis and release. *International Journal of Hematology* **59**, 233–255.

Lindau, M. & Neher, E. (1988). Patch-clamp techniques for time-resolved capacitance measurements in single cells. *Pflügers Archiv* **411**, 137–146.

Lindau, M., Nusse, O., Bennet, J. & Cromwell, O. (1993). The membrane fusion events in degranulating guinea pig eosinophils. *Journal of Cell Science* **104**, 203–210.

Lupu, C., Goodwin, C. A., Westmuckett, A. D., Emeis, J. J., Scully, M. F., Kakkar, V. V. & Lupu, F. (1997). Tissue factor pathway inhibitor in endothelial cells colocalizes with glycolipid microdomains/caveolae. Regulatory mechanism(s). of the anticoagulant properties of the endothelium. *Arteriosclerosis Thrombosis and Vascular Biology* **17**, 2964–2974.

Lupu, C., Lupu, F., Dennehy, U., Kakkar, V. V. & Scully, M. F. (1995). Thrombin induces the redistribution and acute release of tissue factor pathway inhibitor from specific granules within human endothelial cells in culture. *Arteriosclerosis Thrombosis and Vascular Biology* **15**, 2055–2062.

McNeil, P. L. & Steinhardt, R. A. (1997). Loss, restoration, and maintenance of plasma membrane integrity. *Journal of Cell Biology* **137**, 1–4.

McNiff, J. M. & Gil, J. (1983). Secretion of Weibel-Palade bodies observed in extra-alveolar vessels of rabbit lung. *Journal of Applied Physiology* **54**, 1284–1286.

Mann, K. G. (1997). Thrombosis: theoretical considerations. *American Journal of Clinical Nutrition* **65**, 1657S–1664S.

Neher, E. & Marty, A. (1982). Discrete changes of cell membrane capacitance observed under conditions of enhanced secretion in bovine adrenal chromaffin cells. *Proceedings of the National Academy of Science of the USA* **79**, 6712–6716.

Nusse, O., Serrander, L., Lew, D. P. & Krause, K. -H. (1998). Ca^{2+}-induced exocytosis in individual human neutrophils: high- and low-affinity granule populations and submaximal responses. *EMBO Journal* **17**, 1279–1288.

Ogden, D., Khodakhah, K., Carter, T., Thomas, M. & Capiod, T. (1995). Analogue computation of transient changes of intracellular free calcium concentration with the low affinity Ca^{2+} indicator furaptra during whole cell patch clamp recording. *Pflügers Archiv* **49**, 587–591.

Ozaka, T., Doi, Y., Kayashima, K. & Fujimoto, S. (1997). Weibel-Palade bodies as a storage site of calcitonin gene-related peptide and endothelin-1 in blood vessels of the rat carotid body. *Anatomical Records* **247**, 388–394.

Richardson, M., Tinlin, S., De Reske, M., Webster, S., Senis, Y. & Giles, A. R. (1994). Morphological alterations in endothelial cells with the release of von Willebrand factor after thrombin generation *in vivo*. *Arteriosclerosis and Thrombosis* **14**, 990–999.

Russell, F. D., Skepper, J. N. & Davenport, A. P. (1998*a*). Human endothelial cell storage granules: a novel intracellular site for isoforms of the endothelin-converting enzyme. *Circulation Research* **83**, 314–321

Russell, F. D., Skepper, J. N. & Davenport, A. P. (1998*b*). Evidence using immunoelectron microscopy for regulated and constitutive pathways in the transport and release of endothelin. *Journal of Cardiovascular Pharmacology* **31**, 424–430

Scepek, S. & Lindau, M. (1993). Focal exocytosis by eosinophils – compound exocytosis and cumulative fusion. *EMBO Journal* **12**, 1811–1817.

Schaumburg-Lever, G., Gehring, B. & Kaiserling, E. (1994). Ultrastructural localization of factor XIIIa. *Journal of Cutaneous Pathology* **21**, 129–134.

Schneider, S. W., Storck, J., Reinhardt, J., Niemeyer, A., Ossig, R. & Oberleithner, H. (2000). Dynamics of exocytosis imaged by atomic force and laser scanning microscopy. *Pflügers Archiv* **439**, 501–505.

Scrutton, M. C & Pearson, J. D. (1989). Ca^{2+}-driven prostacylin synthesis and von Willebrand factor secretion in electropermeabilised endothelial cells. *British Journal of Pharmacology* **97**, 420P.

Sigworth, F. J. & Sine, S. M. (1987). Data transformations for improved display and fitting of single-channel dwell time histograms. *Biophysical Journal* **52**, 1047–1054.

Sillén, L. G. & Martell, A. E. (1971). *Stability constants supplement 1. Special publication 25*, pp. 650–654. The Chemical Society, London.

Stern, D., Brett, J., Harris, K. & Nawroth, P. (1986). Participation of endothelial cells in the Protein C-Protein S anticoagulant pathway: the synthesis and release of protein S. *Journal of Cell Biology* **102**, 1971–1978.

Terasaki, M., Miyake, K. & McNeil, P. L. (1997). Large plasma membrane disruptions are rapidly resealed by Ca^{2+}-dependent vesicle-vesicle fusion events. *Journal of Cell Biology* **139**, 63–74.

Ueda, H, Doi, Y., Sakamoto, Y., Hamasaki, K., Fujimoto, S. (1992). Simultaneous localization of histamine and factor VIII-related antigen in the endothelium of the human umbilical vein. *Anatomical Record* **23**, 257–261.

Utgaard, J. O., Jahnsen, F. L., Bakka, A., Brandtzaeg, P. & Haraldsen, G. (1998). Rapid secretion of prestored interleukin 8 from Weibel-Palade bodies of microvascular endothelial cells. *Journal of Experimental Medicine* **188**, 1751–1756.

Verhage, M., McMahon, H. T., Ghijsen, W. E., Boomsma, F., Scholten, G., Wiegant, V. M. & Nicholls, D. G. (1991). Differential release of amino acids, neuropeptides, and catecholamines from isolated nerve terminals. *Neuron* **6**, 517–524.

Wagner, D. D. (1990). Cell biology of von Willebrand factor. *Annual Review of Cell Biology* **6**, 217–246.

Weibel, E. R. & Palade, G. F. (1964). New cytoplasmic components in arterial endothelial. *Journal of Cell Biology* **23**, 101–112.

Zupančič, G., Kocmur, L., Veranic, P., Grilc, S., Kordas, M. & Zorec, R. (1994). The separation of exocytosis from endocytosis in rat melanotroph membrane capacitance records. *Journal of Physiology* **480**, 539–552.

Acknowledgements

This work was funded by the British Heart Foundation and the MRC. We would like to thank Drs David Trentham and Gordon Reid for providing DM-nitrophen, and Dr Nicholai Kiskin for help with the equilibrium calculations for the calcium-DM-nitrophen solutions.

Supplementary material

The online version of this paper can be found at:

http://www.jphysiol.org/cgi/content/full/544/3/741

and contains supplementary material. It is a description of the method of analysis used for detection of discrete steps in C_m due to exocytosis and endocytosis, and the influence of p-p noise on the resolution of detection of C_m steps. It also includes a summary of the distributions of p–p noise for recordings used for the histogram construction of Fig. 4 of the paper.